J|A|C|S

ARTICLES

Published on Web 08/05/2003

DFT Computational Study of the Mechanism of Allyl Halides Carbonylation Catalyzed by Nickel Tetracarbonyl

Andrea Bottoni,*,† Gian Pietro Miscione,† Juan J. Novoa,*,‡ and Xavier Prat-Resina§

Contribution from the Dipartimento di Chimica "G. Ciamician", Universita' di Bologna, via Selmi 2, 40126 Bologna, Italy, Department de Quimica Fisica, Facultat de Quimica, Universitat de Barcelona, Av. Diagonal 647, 08028-Barcelona, Spain, and Unitat de Quimica Fisica, Department de Quimica, Universitat Autonoma de Barcelona, 08193 Bellaterra, Barcelona, Spain

Received February 10, 2003; E-mail: andrea@ciamserv.ciam.unibo.it.; novoa@qf.ub.es.

Abstract: A theoretical investigation at the DFT(B3LYP) level on the carbonylation reaction of allyl bromide catalyzed by nickel tetra-carbonyl $Ni(CO)_4$ is discussed. The computational results show the following: (i) Three main steps characterize the catalytic cycle: (a) an oxidative addition step, (b) a carbonylation step, and (c) a reductive elimination step where the acyl product is obtained and the catalyst is regenerated. (ii) Both $Ni(CO)_3$ and $Ni(CO)_4$ complexes can behave as "active" catalytic species. (iii) The oxidative addition leads to the formation of either η^3 or η^1-allyl nickel complexes, which are involved in a fast equilibrium. (iv) The carbonylation occurs much more easily on the η^1 than on the η^3 intermediates.

Introduction

The carbonylation of allyl halides catalyzed by transition metals represents a powerful synthetic tool to obtain β-γ-unsaturated acyl derivatives,[1] and a number of papers, where different transition metal complexes are used as catalysts, have appeared in the literature.[1−16] The carbonylation of allyl halides can be catalyzed by nickel tetracarbonyl $Ni(CO)_4$[2,11−19] and it was first reported by Chiusoli.[2,11] This reaction can be carried out under mild conditions i.e., room temperature and atmospheric or low (2−3 atm) CO pressures.[13] At higher pressures, the reaction is suppressed, unless the temperature is also raised, whereas at lower pressures the dimerization of the allyl groups is favored. When inert solvents, such as ethers or aromatic compounds, are used, the reaction products are acyl halides. In alcohol and other solvents, the reaction proceeds up to the formation of the corresponding acids and esters, depending on the media. The nickel tri-carbonyl complex $Ni(CO)_3$, in equilibrium with the $Ni(CO)_4$ species, is postulated to represent the "active" form of the catalyst.[20] However, because the decomposition of $Ni(CO)_4$ into $Ni(CO)_3$ and CO is an endothermic process (by 22.1 kcal mol^{-1} in *n*-hexane solutions[21] and by 35 kcal mol^{-1} when measured using calorimetric techniques[22]), only a small amount of $Ni(CO)_3$ should be available in the reaction medium.

During the last two decades, the nickel catalyzed carbonylation has lost some of its popularity among the chemical community mainly because of the hazardous nature of $Ni(CO)_4$. It has been replaced in many cases by palladium catalyzed carbonylation[3−10] even if this reaction has the disadvantage of requiring a very high carbon monoxide pressure. However, quite recently the use of nickel complexes has attracted again much interest since alternative techniques have been proposed that avoid the direct manipulation of the toxic $Ni(CO)_4$. This procedure has been applied by Moreto and co-workers[18,19] to the Ni-mediated cyclocarbonylation of allyl halides and alkynes, a reaction reported some time ago by Chiusoli.[13,15] These authors have shown that cyclopentanones can be efficiently and selectively obtained without any handling of nickel carbonyl by preparing the π-allyl Ni complex (the suggested key species of the process) in the way suggested by Mackenzie et al.[23] (i.e., from $Ni(COD)_2$, acryladehydes and Me_3SiCl). This renewed

† Dipartimento di Chimica "G. Ciamician", Universita' di Bologna.
‡ Department de Quimica Fisica, Facultat de Quimica, Universitat de Barcelona.
§ Unitat de Quimica Fisica, Department de Quimica, Universitat Autonoma de Barcelona.

(1) Beller, M.; Cornilis. B.; Frohning, C. D.; Kohlpaintner, C. W. *J. Mol. Catal.* **1995**, *104*, 17.
(2) Chiusoli, G. P. *Chim. Ind.* **1959**, *41*, 503.
(3) Tsuji, J.; Morikawa, M.; Kiji, J. *Tetrrahedron Lett.* **1963**, 1811.
(4) Joo, F.; Alper, H. *Organometallics* **1985**, *4*, 1775. Murahashi, S.-I.; Imada, Y.; Taniguchi, Y.; Higashiura, S. *Tetrrahedron Lett.* **1988**, *29*, 4945.
(5) Yamamoto, A. *Bull. Chem. Soc. Jpn.* **1995**, *68*, 433.
(6) Jiang, H.; Xu, Y.; Liao, S.; Yu, D.; Chen, H.; Li, X. *J. Mol. Catal. A: Chemical* **1998**, *130*, 79.
(7) Bertoux, F.; Monflier, E.; Castanet, Y.; Mortreux, A. *J. Mol. Catal. A: Chemical* **1999**, *143*, 11.
(8) Grigg, R.; Liu, A.; Shaw, D.; Suganthan, S.; Woodall, D. E.; Yoganathan, G. *Tetrrahedron Lett.* **2000**, *41*, 7125.
(9) Bio, M. M.; Leighton, L. *Organic Lett.* **2000**, *2*, 2905.
(10) El. Houssame, S.; El. Firdoussi, L.; Allaoud, S.; Karim, A. Castanet, Y.; Mortreux, A. *J. Mol. Catal. A: Chemical* **2001**, *168*, 15.
(11) Chiusoli, G. P. *Angew. Chem.* **1960**, *72*, 74.
(12) Heck, R. F. *J. Am. Chem. Soc.* **1963**, *85*, 2013.
(13) Chiusoli, G. P.; Cassar, L. *Angew. Chem., Int. Ed. Engl.* **1967**, *6*, 124.
(14) Heck, R. F. *Acc. Chem. Res.* **1969**, *2*, 10.
(15) Chiusoli, G. P. *Acc. Chem. Res.* **1973**, *6*, 422.
(16) Kuhlmann, E. J.; Alexander, J. J. *Coord. Chem. Rev.* **1980**, *33*, 195.
(17) Camps, F.; Coll, J.; Moreto, J. M.; Torras, J. *J. Org. Chem.* **1989**, *54*, 1969.
(18) Pages, L.; Llebaria, A.; Camps, F.; Molins, E.; Miravitlles, C.; Moreto, J. M. *J. Am. Chem. Soc.* **1992**, *114*, 10 449.
(19) Garcia-Gomez, G.; Moreto, J. M. *J. Am. Chem. Soc.* **1999**, *121*, 878.
(20) Bernardi, F.; Bottoni, A.; Nicastro, M.; Rossi, I.; Novoa, J.; Prat, X. *Organometallics* **2000**, *19*, 2170.
(21) Day, J. P.; Pearson, R. G.; Basolo, F. *J. Am. Chem. Soc.* **1968**, *90*, 6933.
(22) Cotton, Ficher, Wilkinson, *J. Am. Chem. Soc.* **1959**, *81*, 100.
(23) Johnson, J. R.; Tully, P. S.; Mackenzie, P. B.; Sabat, M. *J. Am. Chem. Soc.*, **1991**, *113*, 6172. Grisso, B. A.; Johnson, J. R.; Mackenzie, P. B. *J. Am. Chem. Soc.* **1992**, *114*, 5160.

10.1021/ja030100f CCC: $25.00

Scheme 1

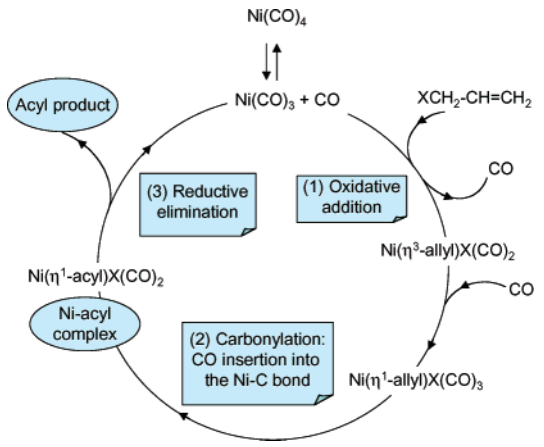

Scheme 2

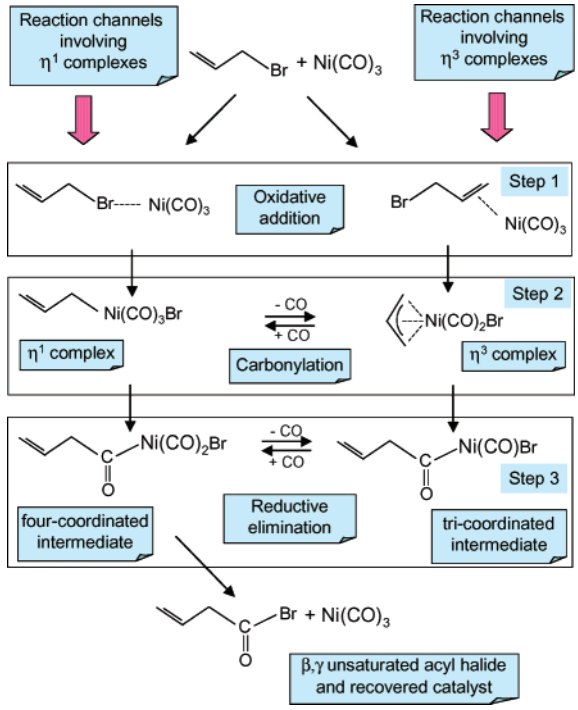

interest for nickel catalyzed carbonylations has prompted us to consider in detail the mechanism of this reaction. Also, it is worth to outline that only a few theoretical papers on the carbonylation catalyzed by $Ni(CO)_4$ are available in the literature[20,24−26] and, as far as we know, no papers have appeared on the nickel catalyzed carbonylation of allyl halides.

A schematic representation of the commonly postulated catalytic cycle for the carbonylation of allyl halides is reported in Scheme 1. The mechanism consists of three major steps: (1) The oxidative addition of allyl halides $XCH_2-CH=CH_2$ to nickel to form η^3 and/or η^1-allyl complexes. (2) The carbonylation step where a CO molecule inserts into a carbon−nickel bond and nickel-acyl complexes are obtained. (3) The reductive elimination, which affords the acyl product (acyl halide) with the regeneration of the catalyst.

In light of the experimental evidence[11−19] published in the literature, it is possible to propose a much more detailed mechanism (see Scheme 2). The structures of the possible intermediates involved in the various reaction paths are based on those suggested in the literature. In this scheme, the $Ni(CO)_3$ is assumed to be active catalytic species. The initial oxidative addition step (1) could proceed either via an attack of the terminal CC double bond of the allyl halide on the metal, or via a direct attack of the halogen. In the former case we have the formation of η^3-allyl complexes, whereas in the latter, the reaction leads to η^1-allyl complexes. The experiments suggest the existence of a possible equilibrium between these two complexes. This equilibrium requires the addition or the expulsion of a CO ligand from the metal coordination sphere. The carbonylation (step 2) could occur, in principle, either on the η^3 or the η^1-allyl species. Three-coordinated and four-coordinated nickel-acyl complex intermediates are obtained in the former and latter case, respectively. Reductive elimination (step 3) from the four-coordinated complexes leads to $\beta,\gamma-$unsaturated acyl halides and the regenerated catalyst. As the experimental data of Scheme 2 suggest that most of the catalyst is present in the reaction medium as $Ni(CO)_4$, a similar scheme starting from $Ni(CO)_4$ and involving equivalent steps should be also considered.

Despite being one of the first useful examples of allyl halide carbonylation of technological interest, various mechanistic details (partially reported in Scheme 2) have not been elucidated yet, and many questions still remain unanswered. What is, for instance, the real "active" catalytic species; $Ni(CO)_3$, which is present in the reaction medium in small amount, or the tetracarbonyl nickel complex $Ni(CO)_4$? Are π-complexes involved in the process? Does carbonylation occur on the η^3 or η^1 species? Are the η^3 and η^1 complexes in equilibrium? What is the rate-determining step of the process?

In the present paper, to answer these and other questions and to obtain a detailed mechanistic picture, the carbonylation reaction of allyl halides catalyzed by nickel tetra-carbonyl has been investigated in detail at the DFT level. The model-system is formed by an allyl bromide molecule. We have studied its reaction with $Ni(CO)_4$ and $Ni(CO)_3$ because, as mentioned before, both complexes, in principle, can play the role of "active" catalyst.

2. Computational Procedure. All the DFT computations reported here have been performed with the Gaussian 98[27] series of programs using the nonlocal hybrid Becke's three-parameter exchange functional[28,29] denoted as B3LYP. Following the Gaussian formalism, this functional can be written as follows

$$0.80E(S)_X + 0.20E(HF)_X + 0.72E(B88)_X + 0.19E(LOCAL)_C + 0.81E(NON\text{-}LOCAL)_C$$

(24) De Angelis, F.; Re, N.; Sgamellotti, A.; Selloni, A.; Weber, J.; Floriani, C. *Chem. Phys. Lett.* **1998**, *291*, 57.
(25) De Angelis, F.; Sgamellotti, A. *Organometallics* **2000**, *19*, 4104.
(26) Carbo, J. J.; Bo, C.; Poblet, J. M.; Moreto, J. M. *Organometallics* **2000**, *19*, 3516.
(27) Frisch, M. J.; Trucks, G. W.; Schlegel, H. B.; Scuseria, G. E.; Robb, M. A.; Cheeseman, J. R.; Zakrzewski, V. G.; Montgomery, J. A., Jr.; Stratmann, R. E.; Burant, J. C.; Dapprich, S.; Millam, J. M.; Daniels, A. D.; Kudin, K. N.; Strain, M. C.; Farkas, O.; Tomasi, J.; Barone, V.; Cossi, M.; Cammi, R.; Mennucci, B.; Pomelli, C.; Adamo, C.; Clifford, S.; Ochterski, J.; Petersson, G. A.; Ayala, P. Y.; Cui, Q.; Morokuma, K.; Malick, D. K.; Rabuck, A. D.; Raghavachari, K.; Foresman, J. B.; Cioslowski, J.; Ortiz, J. V.; Stefanov, B. B.; Liu, G.; Liashenko, A.; Piskorz, P.; Komaromi, I.; Gomperts, R.; Martin, R. L.; Fox, D. J.; Keith, T.; Al-Laham, M. A.; Peng, C. Y.; Nanayakkara, A.; Gonzalez, C.; Challacombe, M.; Gill, P. M. W.; Johnson, B. G.; Chen, W.; Wong, M. W.; Andres, J. L.; Head-Gordon, M.; Replogle, E. S.; Pople, J. A. *Gaussian 98*; Gaussian, Inc.: Pittsburgh, PA, 1998.
(28) Becke, A. D. *J. Chem. Phys.* **1993**, *98*, 1372, 5648.
(29) Stephens, P. J.; Devlin, F. J.; Chabalowsky, C. F.; Frisch, M. J. *J. Phys. Chem.* **1994**, *98*, 11 623.

where $E(S)_X$ is the Slater exchange,[30] $E(HF)_X$ the Hartree−Fock exchange, $E(B88)_X$ represents the Becke's 1988 nonlocal exchange functional corrections,[31] $E(LOCAL)_C$ corresponds to the Vosko, Wilk, and Nusair local correlation functional[32] and $E(NON\text{-}LOCAL)_C$ to the correlation functional of Lee, Yang, and Parr ($E(LYP)_C$),[33] which includes both local and nonlocal terms. This functional has been demonstrated to be able of providing a reliable description (structures and energies) of transition metal complexes and of the potential surfaces associated with catalytic processes.[20,24,25,34−37] In particular, in refs 20, 24, 25, and 37 examples are reported which show that the B3LYP functional is adequate to describe oxidative addition, carbonylation and reductive elimination steps occurring in the catalytic cycle. The geometry of the various critical points on the reaction surface has been fully optimized with the gradient method available in Gaussian 98 using the DZVP basis set,[38] which is a Local Spin Density (LSD)-optimized basis set of double-ζ quality in the valence shell plus polarization functions. A computation of the harmonic vibrational frequencies has been carried out to determine the nature of each critical point. To check the reliability of the DZVP basis, the structure of the most important critical points has been re-optimized using a more accurate basis set: the 6-31G* basis[27] for carbon and hydrogen atoms and the 6-311G* basis[27] for the metal and the bromine (6-31G*/6-311G* basis).

To roughly evaluate the effect of the solvent, in some cases, we carried out single-point computations on the gas-phase optimized structures using the Polarized Continuous Model (PCM)[39] method available in Gaussian 98.

3. Results and Discussion

In this section, we discuss in detail the singlet potential energy surface associated with the various steps of the catalytic cycle of Scheme 2.

A. Mechanism of the Oxidative Addition: Formation of η^3 Complexes. The energy profile for this process is represented in Figure 1, whereas the structures of the various critical points located on the potential surface, with the values of the most relevant geometrical parameters, are reported in Figure 2. From the energy profile it is evident that the oxidative addition involves a preliminary η^2 π-complex (M_1), where the terminal CC double bond interacts with the nickel atom. If we consider $Ni(CO)_3$ as the "active" form of the catalyst, M_1 forms without any barrier and is 10.1 kcal mol^{-1} lower than reactants ($Ni(CO)_3$ + allyl bromide). In M_1, the lengths of the two Ni−C bonds are 2.225 and 2.198 Å. The CC bond has slightly lost its double bond character and is now 1.375 Å (1.339 Å in free allyl bromide). On the other hand, if we consider $Ni(CO)_4$ as "active" species, the formation of M_1 requires the overcoming of a barrier of 19.4 kcal mol^{-1} (transition state TS_1). The barrier is associated to the expulsion of a CO ligand as the allyl bromide enters the metal coordination sphere. A rotation around the CC single bond leads from M_1 to a new and less stable (by 2.5 kcal mol^{-1}) intermediate M_2, where the bromine atom is much closer to the metal atom (Br−Ni distance = 3.860 Å). The transition state for the M_1 to M_2 pathway is 5.0 kcal mol^{-1} higher than M_1, although it is still below the energy of the initial $Ni(CO)_3$ + allyl bromide reactants. Once in M_2, it is possible for the bromine atom to migrate from the carbon to the metal.

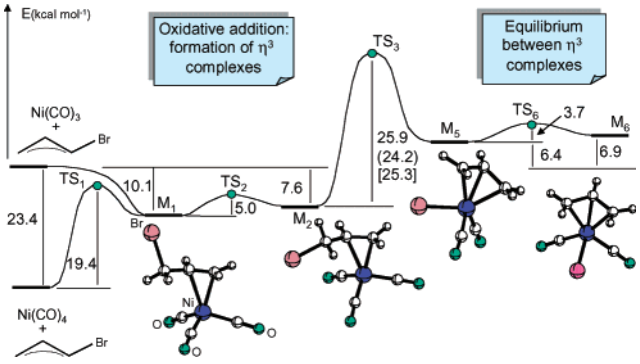

Figure 1. Energy profile for the oxidative addition leading to η^3 complexes. (Energies are in kcal mol^{-1}). Values in parentheses have been obtained at the 6-31G*/6-311G* level. Values in square brackets include solvent effects.

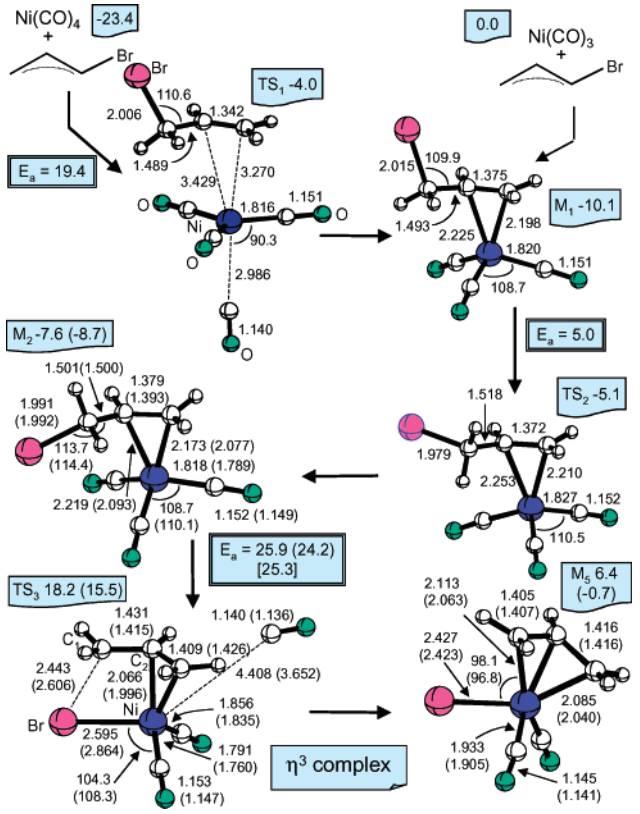

Figure 2. Schematic representation of the structures of the critical points M_1, TS_1, M_2, TS_2, TS_3, and M_5. Bond lengths are in Ångstroms and angles in degrees. The energies (kcal mol^{-1}) are relative to reactants ($Ni(CO)_3$ + allylbromide). The absolute energy of reactants is: −4539.1862 au (DZVP basis); −4539.7511 au (6-31G*/6-311G* basis). Values in parentheses have been obtained at the 6-31G*/6-311G* level. Values in square brackets include solvent effects.

(30) Hohenberg, P.; Kohn, W. *Phys. Rev. B* **1964**, *136*, 864. Kohn, W.; Sham, L. J. *Phys. Rev. A* **1965**, *140*, 1133.
(31) Becke, A. D. *Phys. Rev.* **1988**, *A38*, 3098.
(32) Vosko, S. H.; Wilk, L.; Nusair, M. *Can. J. Phys.* **1980**, *58*, 1200.
(33) Lee, C.; Yang, W.; Parr, R. G. *Phys. Rev.* **1988**, *B37*, 785. Miehlich, A.; Savin, A.; Stoll, H.; Preuss, H. *Chem. Phys. Lett.* **1989**, *157*, 200.
(34) Bernardi, F.; Bottoni, A.; Miscione, G. P. *J. Am. Chem. Soc.* **1997**, *119*, 12 300.
(35) Bernardi, N.; Bottoni, A.; Casolari, S.; Tagliavini, E. *J. Org. Chem.* **2000**, *65*, 4783.
(36) Bottoni, A.; Perez Higueruelo, A.; Miscione, G. P. *J. Am. Chem. Soc.* **2002**, *124*, 5506.
(37) Bernardi, F.; Bottoni, A.; Garavelli, M. *Quant. Struct.-Act. Relat.* **2002**, *21*, 128.
(38) Godbout, N.; Salahub, D. R.; Andzelm, J.; Wimmer, E. *Can. J. Chem.* **1992**, *70*, 560. **UniChem DGauss**, Version 2.3.1, 1994, Cray Research, Inc.
(39) Miertus, S.; Scrocco, E.; Tomasi, J. *J. Chem. Phys.* **1981**, *55*, 117. Miertus, S.; Tomasi, J. *J. Chem. Phys.* **1982**, *65*, 239.

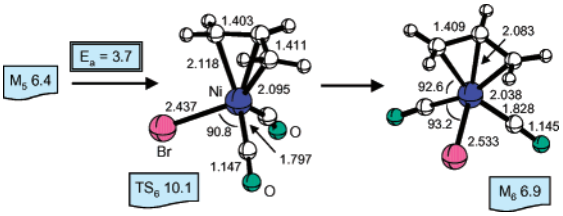

Figure 3. Schematic representation of the structures of the critical points TS_6 and M_6. Bond lengths are in Ångstroms and angles in degrees. The energies (kcal mol^{-1}) are relative to reactants ($Ni(CO)_3$ + allylbromide).

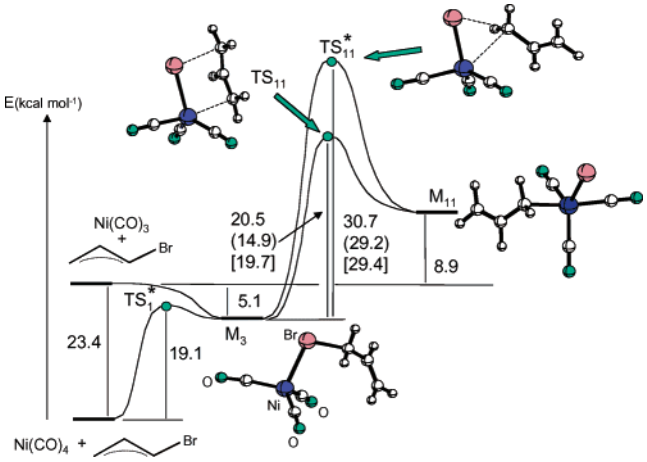

Figure 4. Energy profile for the oxidative addition leading to η^1 complexes. (Energies are in kcal mol^{-1}). Values in parentheses have been obtained at the 6-31G*/6-311G* level. Values in square brackets include solvent effects.

This leads to the η^3−complex intermediate M_5, placed 6.4 kcal mol^{-1} higher than the asymptotic limit ($Ni(CO)_3$ + allyl bromide). In this way, the bromine atom replaces one CO ligand in the metal coordination sphere. In M_5 the two CC bond distances have similar values (1.416 and 1.405 Å) in agreement with the complete delocalization of the allyl π system. This transformation occurs via transition state TS_3 and requires the overcoming of a rather large barrier (25.9 kcal mol^{-1}), which is mainly due to the breaking of the nickel−carbon bond when the CO ligand is expelled. The migration of the halogen is evident in the schematic representation of TS_3 (Figure 2). Here, the bromine atom is halfway between the carbon and the metal, (the C_1−Br and Ni−Br distances are 2.443 and 2.595 Å, respectively), whereas the new forming Ni−C_1 bond is 2.524 Å. The transition vector obtained from the frequency computations on TS_3 is dominated by the C_1−Br and Ni−Br distances and the C_2−Ni−Br angle.

A second η^3-complex (M_6), almost degenerate to M_5 (only 0.5 kcal mol^{-1} lower in energy), exists on the potential surface. This complex, which can be obtained from M_5 through transition state TS_6 with a barrier of 3.7 kcal mol^{-1}, has C_{2v} symmetry and, thus, identical values of the two C−C bonds (1.409 Å) and the two external Ni−C bonds (2.038 Å). A picture of M_6 and TS_6 is reported in Figure 3.

B. Alternative Oxidative Addition: Direct Attack of Br on the Nickel Atom. We have demonstrated the existence of an alternative oxidative addition path whose energy profile is reported in Figure 4. This reaction channel corresponds to a direct attack of the bromine atom on the $Ni(CO)_3$ complex and leads to a preliminary intermediate M_3, where the halogen is simultaneously bonded to the allyl carbon and the metal (see

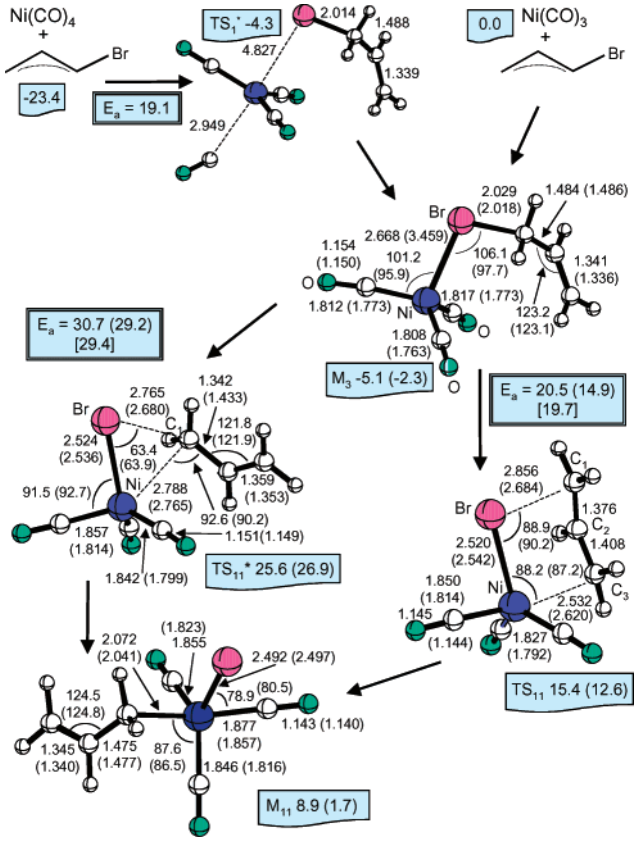

Figure 5. Schematic representation of the structures of the critical points TS_1*, M_3, TS_{11}*, TS_{11}, and M_{11}. Bond lengths are in Ångstroms and angles in degrees. The energies (kcal mol^{-1}) are relative to reactants ($Ni(CO)_3$ + allylbromide). Values in parentheses have been obtained at the 6-31G*/6-311G* level. Values in square brackets include solvent effects.

Figure 5). Because $Ni(CO)_3$ has an unsaturated coordination sphere, no ligands must be expelled, and the formation of M_3, which is 5.1 kcal mol^{-1} lower than that of the reactants, does not require any energy barrier. As discussed in the previous section, if we assume $Ni(CO)_4$ as an "active species", the formation of M_3 is characterized by an activation energy of 19.1 kcal mol^{-1} (transition state TS_1*). Two separate channels lead from M_3 to the η^1−allyl-nickel complex M_{11}. One requires the overcoming of a large barrier (30.7 kcal mol^{-1}) and corresponds to a migration of the allyl fragment from the halogen to the metal (transition state TS_{11}*). This pathway is confirmed by the relative weights of the components of the transition vector, which is dominated by the C_1−Br and C_1−Ni distances. The other pathway is much more interesting since a significantly lower activation barrier of 20.5 kcal mol^{-1} characterizes it. In this case, the allyl fragment slides along a direction parallel to the Ni−Br bond (transition state TS_{11}) and the carbon originally bonded to bromine becomes the terminal methylene carbon in the final complex M_{11}. Accordingly, the most important components of the transition vector for TS_{11} are the two C_1−Br and C_3−Ni distances. M_{11} is a five-coordinated nickel species, which is 8.9 kcal mol^{-1} higher than the asymptotic limit. Schematic representations of TS_{11}*, TS_{11}, and M_{11} are given in Figure 5. The entity of the barrier found for TS_{11} indicates that the direct oxidative addition path can be highly competitive with that leading to η^3 complexes.

C. η^3 and η^1 Species are in Equilibrium. The η^3 complexes M_5 and M_6 can be converted to η^1 complexes after coordination

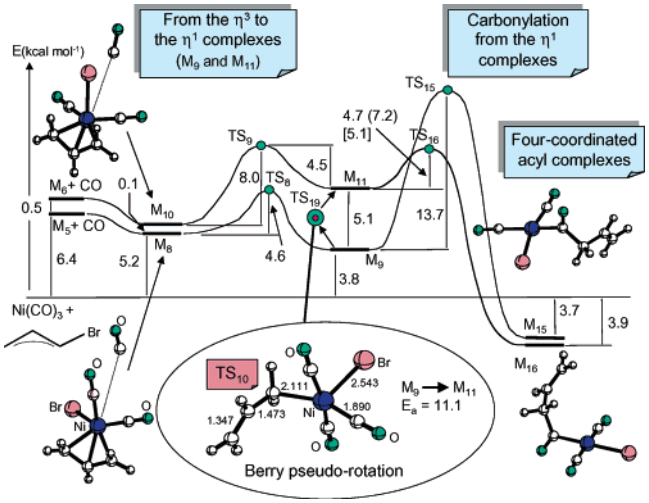

Figure 6. Energy profile for the equilibrium $\eta^3 \rightarrow \eta^1$ (left side) and the carbonylation involving η^1 complexes (right side). (Energies are in kcal mol^{-1}). The structure of TS_{10} is reported in the enlargement. Values in parentheses have been obtained at the 6-31G*/6-311G* level. Values in square brackets include solvent effects.

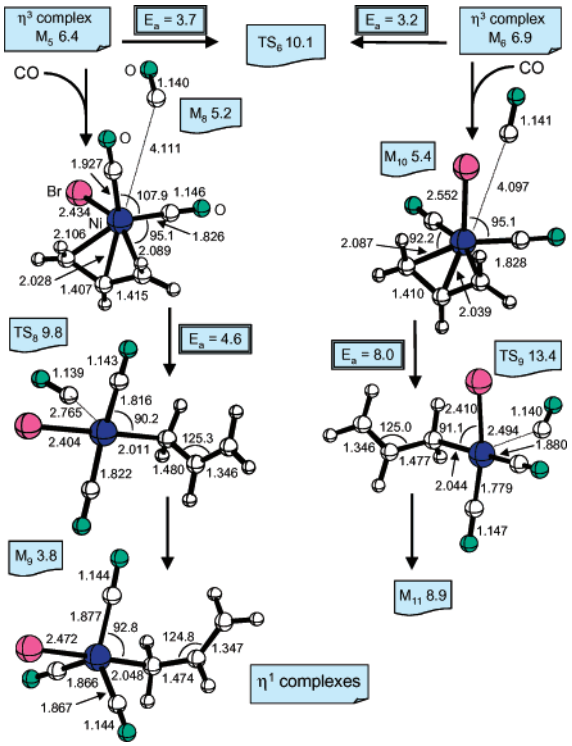

Figure 7. Schematic representation of the structures of the critical points M_8, M_{10}, TS_8, TS_9, and M_9. Bond lengths are in Ångstroms and angles in degrees. The energies (kcal mol^{-1}) are relative to reactants ($Ni(CO)_3$ + allylbromide).

of an additional CO ligand. The corresponding energy profile is represented in Figure 6 and the detailed structures of the various critical points are shown in Figure 7 (its top part just highlights the equilibrium between M_5 and M_6). The addition of a CO ligand to M_5 or M_6 leads to the formation of two preliminary long-range complexes M_8 and M_{10}. These species are slightly more stable than the starting η^3 complexes M_5 or M_6, (1.2 and 1.6 kcal mol^{-1} more stable than M_5 + CO and M_6 + CO, respectively). The weak bonding interaction between CO and the metal is characterized in both cases by a Ni−C distance of 4.111 Å. M_8 and M_{10} can be converted to the five-coordinated η^1 complexes M_9 and M_{11} (see also Figure 5) by overcoming a barrier of 4.6 (transition state TS_8) and 8.0 kcal mol^{-1} (transition state TS_9), respectively. In the two transition states the metal atom has approximately a square planar structure where the incoming CO is approaching the metal along a direction orthogonal to the molecular plane. The distance between the metal and the carbon of the approaching CO is the dominant component of the transition vectors computed for both transition states. The newly forming nickel−carbon(CO) bond is 2.765 and 2.494 Å in TS_8 and TS_9, respectively. In both cases, the metal is bonded to one terminal carbon of the allyl moiety. This atom has sp^3 hybridization, and consequently, the central CC bond is basically a single bond (about 1.48 Å), whereas the terminal CC bond definitely has a double bond character (about 1.35 Å). The two final η^1 complexes M_9 and M_{11} are five-coordinated species with a distorted trigonal bi-pyramid structure. In M_9, which is 1.4 kcal mol^{-1} lower than M_8 and 5.1 kcal mol^{-1} lower than M_{11}, the bromine and the allyl fragment are in axial positions, while in M_{11}, 3.6 kcal mol^{-1} higher than M_{10}, the axial Br atom is replaced by a CO molecule. A comparison of the two energy profiles (thermodynamic stability of the product and kinetic barriers) indicates that the most convenient way to carry out the transformation $\eta^3 \rightarrow \eta^1$ is represented by the channel $M_5 \rightarrow M_8 \rightarrow TS_8 \rightarrow M_9$.

Also, a transition state (TS_{10}) connecting the two five-coordinated complexes M_9 and M_{11} has been located. This transition state is shown in Figure 6 (enlargement on the bottom side) and describes the interchange of bromine and CO from axial to equatorial position (Berry pseudorotation), as pointed out by the corresponding transition vector. TS_{10} is characterized by a nonnegligible lengthening of the bonds between the metal and the two atoms involved in the pseudorotation i.e., Br (Ni−Br = 2.543 Å) and C(CO) (Ni−C = 1.890 Å). The channel connecting M_9 to M_{11} is symbolically indicated in Figure 6, together with the values of the corresponding activation barrier (11.1 kcal mol^{-1}). The reverse barrier ($M_{11} \rightarrow M_9$ transformation) is 6.0 kcal mol^{-1}.

D. Carbonylation Step: Does this Process Occur via η^1 or η^3 Species? The carbonylation process has been investigated for both the η^1 and η^3 complexes discussed in the previous sections. The energy profiles associated with the carbonylation of M_9 and M_{11} (η^1 complexes) are reported on the right-end side of Figure 6, whereas the structures of the corresponding critical points are illustrated in Figure 8. If we consider the more stable η^1 complex M_9, the insertion of a CO ligand into the nickel−carbon bond can be accomplished by overcoming a barrier of 13.7 kcal mol^{-1}. As a matter of fact, the insertion of CO (transition state TS_{15}) is actually a migration of the allyl unit from the metal to the carbon atom of one CO ligand and does not cause any weakening of the nickel−carbon(CO) bond, which, on the contrary, becomes stronger (1.754 Å in TS_{15} and 1.818 Å in M_9). This analysis is in agreement with the form of the computed transition vector whose most important components are the two C_1−Ni and C_1−C(CO) distances and the C_1−Ni−Br angle. Also, inspection of Figure 8 shows that TS_{15} is a reactant-like transition state: the breaking Ni−C bond is still quite strong, its length being 2.276 Å (2.048 Å in M_9) and the new forming C(allyl)−C(CO) bond is only 2.056 Å (1.532 Å in the acyl complex M_{15}).

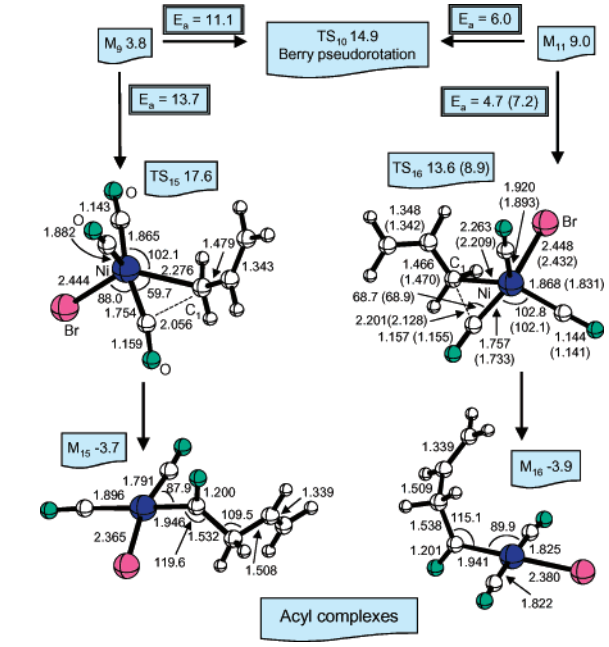

Figure 8. Schematic representation of the structures of the critical points TS_{15}, TS_{16}, M_{15}, and M_{16}. Bond lengths are in Ångstroms and angles in degrees. The energies (kcal mol^{-1}) are relative to reactants ($Ni(CO)_3$ + allylbromide. Values in parentheses have been obtained at the 6-31G*/6-311G* level.

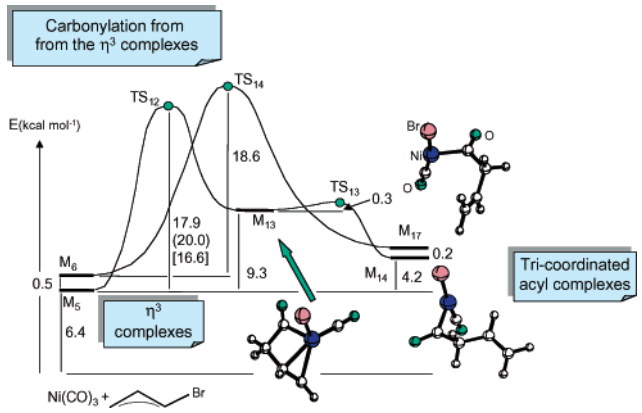

Figure 9. Energy profile for the carbonylation involving η^3 complexes. (Energies are in kcal mol^{-1}). Values in parentheses have been obtained at the 6-31G*/6-311G* level. Values in square brackets include solvent effects.

A similar transition state (TS_{16}) describes the CO insertion occurring on the less stable η^1 complex M_{11}. The computed transition vector (dominant components = C_1-Ni and $C_1-C(CO)$ distances and $C_1-Ni-C(CO)$ angle) again indicates a migration of the allyl moiety. Interestingly, this transition state leads to the acyl complex M_{16} by overcoming a significantly lower activation barrier of 4.7 kcal mol^{-1}. The values of the two insertion barriers and that of the Berry pseudorotation barrier suggest that, for complex M_9, the two-step-process involving first a Berry pseudorotation (TS_{10}, E_a = 11.1 kcal mol^{-1}) and, then, the insertion (TS_{16}, E_a = 4.7 kcal mol^{-1}) can represent an alternative and competitive way to undergo carbonylation.

We have found that the carbonylation can also occur on the η^3 complexes M_5 and M_6 (see Figure 9 for the corresponding energy profiles and Figure 10 for the structures of the various critical points). By overcoming a barrier of 17.9 kcal mol^{-1} (transition state TS_{12}) one goes from M_5 to an intermediate acyl complex M_{13}. The path corresponds again to a migration of the

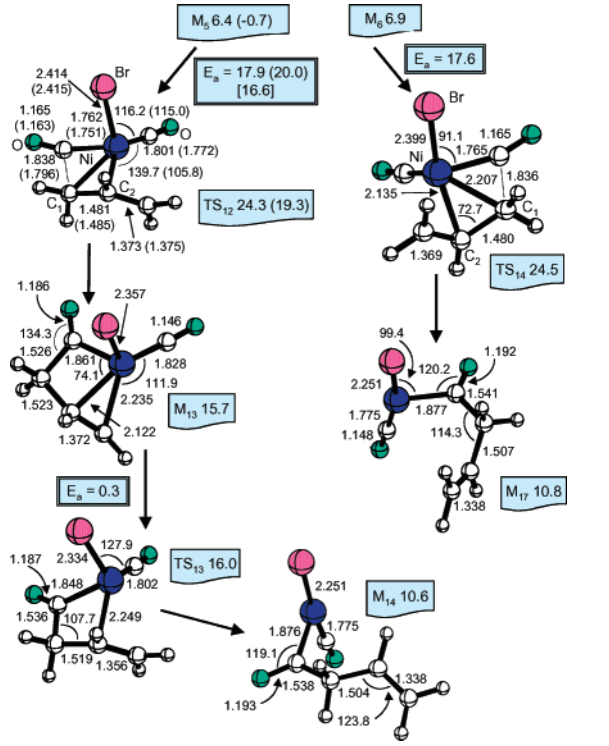

Figure 10. Schematic representation of the structures of the critical points TS_{12}, TS_{14}, M_{13}, M_{17}, TS_{13}, and M_{14}. Bond lengths are in Ångstroms and angles in degrees. The energies (kcal mol^{-1}) are relative to reactants ($Ni(CO)_3$ + allylbromide. Values in parentheses have been obtained at the 6-31G*/6-311G* level. Values in square brackets include solvent effects.

allyl fragment as indicated by the shape of the transition vector, where the largest components are the C_1-Ni and the $C_1-C(CO)$ distances and the $C_2-Ni-C(CO)$ angle. In M_{13}, the insertion process is completed, but the allyl fragment is still interacting with the metal atom via the terminal CC π system. Because of this interaction M_{13} is a cyclic penta-atomic structure with the bromine atom orthogonal to the molecular plane. A very small barrier (only 0.3 kcal mol^{-1} associated with transition state TS_{13}) divides M_{13} from the final tricoordinate acyl complex M_{14}. Because M_{14} has an unsaturated coordination sphere, it is significantly less stable than the four-coordinated acyl complex derived from the η^1 species (10.8 kcal mol^{-1} higher than the asymptotic limit represented by $Ni(CO)_3$ + allylbromide). It is worth noting that the real physical meaning of the very small barrier associated with TS_{13} is arguable. Most likely, it is a computational shortcoming due, perhaps, to a basis set superposition error. Also, we should remember that the underestimation of the energy barriers is a well-known feature of the DFT method.

The carbonylation occurs in a similar way on the M_6 species. Even if in this case no intermediate acyl complex has been located, the barrier required for the insertion (18.6 kcal mol^{-1}), and the corresponding transition state structure (TS_{14}) and transition vector are very similar to those found for M_5. The final three-coordinated acyl complex M_{17} is almost degenerate to M_{14} (only 0.2 kcal mol^{-1} higher) and corresponds to a different conformational arrangement of the acyl moiety. These computational results indicate that the carbonylation is favored when the η^1 complexes are involved.

E. Reductive Elimination Step: Final Acyl Bromide Product and Catalyst Regeneration. We have investigated in detail the reductive elimination process, which produces the final

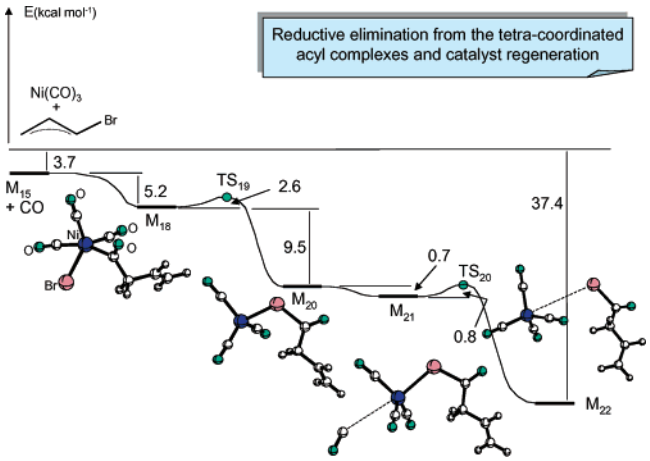

Figure 11. Energy profile for the reductive elimination. (Energies are in kcal mol^{-1}).

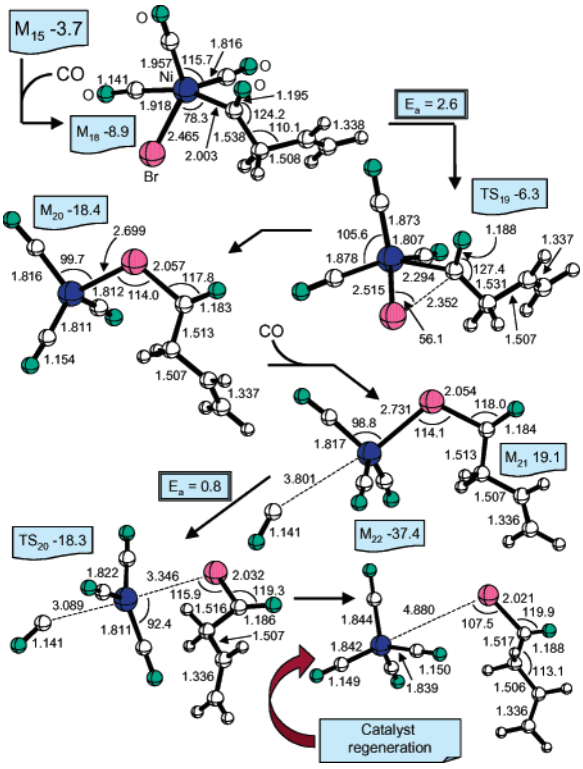

Figure 12. Schematic representation of the structures of the critical points M_{18}, TS_{19}, M_{20}, M_{21}, TS_{20}, and M_{22}. Bond lengths are in Ångstroms and angles in degrees. The energies (kcal mol^{-1}) are relative to reactants ($Ni(CO)_3$ + allylbromide).

β,γ-unsaturated acyl product and regenerates the catalyst. To this purpose, we have considered the process as originating from the four-coordinated nickel acyl complex M_{15}. We have chosen M_{15} instead of M_{16} since the two complexes are isomers (almost degenerate) and we do not expect relevant differences in the reductive elimination. The potential surface is depicted in Figure 11 and the structures of the various critical points are reported in Figure 12.

Following the mechanism represented in these figures, M_{15} can coordinate an additional CO ligand to provide the five-coordinated nickel complex M_{18}, which is 5.2 kcal mol^{-1} more stable. An insertion of the bromine atom into the metal−carbon(acyl) bond occurs easily by overcoming a small barrier of 2.6 kcal mol^{-1} (TS_{19}). This transition state is characterized by a cyclic structure with the bromine atom approximately halfway between nickel and acyl carbon (Ni−Br and Br−C bond distances are 2.515 and 2.352 Å, respectively). It has a reactant-like character, because the nickel−carbon bond (2.294 Å) is only slightly longer (approximately 14%) than in the complex M_{18} (2.003 Å). The resulting species (M_{20}) is again a four-coordinated nickel complex with a bridged bromine among nickel and acyl carbon. This complex can undergo reductive elimination after addition of a new CO molecule. This is a likely event because, in the real experimental conditions, an excess of carbon monoxide is present in the molecular environment. After formation of a long-range complex M_{21}, where the new approaching CO weakly interacts with the metal (nickel−carbon(CO) distance = 3.801 Å), the overcoming of a small barrier of 0.8 kcal mol^{-1} (transition state TS_{20}) gives rise to the final product (β,γ−unsaturated acyl bromide) and the regenerated catalyst in the form of $Ni(CO)_4$ complexes.

F. Solvent Effect and Basis Set Effect. The values of the most relevant energy barriers (E_a) have been re-computed in the presence of the solvent effects and are reported in square brackets in Figures 1, 4, 6, and 9 for the following transformations: (i) $M_2 \rightarrow TS_3$; (ii) $M_3 \rightarrow TS_{11}$; (iii) $M_3 \rightarrow TS_{11}$*; (iv) $M_{11} \rightarrow TS_{16}$; and (v) $M_5 \rightarrow TS_{12}$. The emulated solvent is CH_2Cl_2 (dielectric constant $\epsilon = 8.93$), which is the solvent commonly used in the experiment. The values obtained for the corresponding activation barriers are 25.3, 19.7, 29.4, 5.1, and 16.6 kcal mol^{-1}, respectively. Thus, in all cases, the inclusion of the solvent effects in the computations affects the results only slightly and indicates that the simple gas-phase model used here is adequate for describing this class of reactions.

To validate the results obtained with the DZVP basis set, we have re-optimized the critical points for the above-mentioned transformations using the more accurate 6-31G*/6-311G* basis set (see computational section). The new geometrical parameters and the energy values (relative to reactants: $Ni(CO)_3$ + allylbromide) of the various critical points and the corresponding activation energies are reported in parentheses in the figures. The mechanistic scenario, which stems from these data is very similar to that obtained from the DZVP results. For instance, the barriers involved in the three oxidative addition steps $M_2 \rightarrow TS_3$, $M_3 \rightarrow TS_{11}$, and $M_3 \rightarrow TS_{11}$* become 24.2, 14.9, and 29.2 kcal mol^{-1} (25.9, 20.5, and 30.7 with the DZVP basis). Thus, the direct oxidative addition mechanism (attack of the bromine atom) remains favored. Also, the carbonylation of the η^1−ally-$Ni(CO)_3Br$ species ($M_{11} \rightarrow TS_{16}$, $E_a = 7.2$ kcal mol^{-1}) is again highly favored with respect to that of the η^3−ally-$Ni(CO)_2Br$ intermediate ($M_5 \rightarrow TS_{12}$, $E_a = 20.0$ kcal mol^{-1}).

4. Conclusions

In this paper, we have carried out a theoretical investigation at the DFT(B3LYP) level on the carbonylation reaction of allyl halides catalyzed by nickel tetra-carbonyl. A model-system formed by an allyl bromide molecule reacting either with the $Ni(CO)_3$ or the $Ni(CO)_4$ species, has been considered. The most relevant results obtained in the present study can be summarized as follows:

(i) In agreement with the common mechanistic assumptions, three main steps have been recognized to characterize the catalytic cycle: (1) An oxidative addition step; (2) a carbony-

lation step; and (3) a reductive elimination step where the acyl product is obtained and the catalyst is regenerated.

(ii) It has been demonstrated that the initial oxidative addition can start either from $Ni(CO)_3$ or $Ni(CO)_4$. Thus, both complexes can behave as "active" catalytic species.

(iii) Two main channels for the oxidative addition exist on the reaction surface. One involves the attack of the allyl π system on the metal and leads to the formation of η^3-allyl nickel complexes (η^3-ally-$Ni(CO)_2Br$) by overcoming a barrier of 25.9 kcal mol^{-1}. The other is a direct attack of the bromine on the nickel atom. In this case, a barrier of 20.5 kcal mol^{-1} has been computed and η^1-allyl nickel complexes (η^1-ally-$Ni(CO)_3Br$) are obtained. Thus, at least for the simple model-system used here, the latter reaction pathway is favored. However, because the difference between the two activation barriers is not remarkably large, in principle, in the real experimental conditions (solvent, temperature, pressure), the two reaction pathways could compete in the oxidation addition phase.

(iv) The η^3 and η^1 allyl complexes are involved in a fast equilibrium. The activation barrier for the transformation $M_5(\eta^3) \rightarrow M_9(\eta^1)$ is, in fact, only 4.6 kcal mol^{-1} and that for $M_{11}(\eta^1) \rightarrow M_6(\eta^3)$ is 4.5 kcal mol^{-1}. Thus, even if the easiest way to carry out the oxidative addition is that leading directly to η^1 allyl complexes, both η^1 and η^3 species should be simultaneously present in the reaction medium.

(v) The carbonylation occurs more easily on the η^1 than on the η^3 species as suggested by the relative magnitude of the various activation barriers that are involved. The fastest way to afford the acyl product requires a barrier of only 4.7 kcal mol^{-1} ($M_{11} \rightarrow TS_{16} \rightarrow M_{15}$).

(vi) The general features of the potential surface indicate that the most likely reaction path leading from reactants to the final acyl product is given by the following simple sequence of transformations: (1) oxidative addition and formation of the η^1-ally-$Ni(CO)_3Br$ complex M_{11} (barrier of 20.9 kcal mol^{-1}); and (2) fast carbonylation of the complex M_{11}, which requires a barrier of only 4.7 kcal mol^{-1}. Thus, the oxidative addition would represent the rate-determining step of the reaction. An alternative reaction path can be followed if the oxidative addition leading to the η^3-ally-$Ni(CO)_2Br$ complexes (M_5) becomes competitive. In this case, the following transformations can lead to the final products: (a) Equilibrium between M_5 and the η^1-ally-$Ni(CO)_3Br$ complex M_9 (this requires a barrier of 4.6 kcal mol^{-1}). (b) Isomerization of M_9 to the other η^1 complex M_{11} via a Berry pseudorotation (barrier of 11.1 kcal mol^{-1}). (c) Carbonylation of M_{11} to form the acyl-Ni complex M_{15} (barrier of 4.7 kcal mol^{-1}).

(vii) The solvent effect, which mimics CH_2Cl_2, has a negligible consequence on the activation barriers. This finding suggests that the simple gas-phase model-system used here is reliable to describe this class of catalyzed reactions.

Acknowledgment. We would like to thank the following institutions: (a) Hispano-italian exchange action. J.J.N. CICYT and CIRIT. (b) C.N.R. and M.U.R.S.T. (Progetto Nazionale "Stereoselezione in Sintesi Organica: Metodologie ed Applicazioni") and Bologna University (funds for selected research topics) for the financial support of these researches.

JA030100F